THE AMERICAN SOCIETY OF MECHANICAL ENGINEERS
345 E. 47 St., New York, N.Y. 10017

90-GT-258

Laser Velocimeter Measurements in a Centrifugal Pump with a Synchronously Orbiting Impeller

RONALD J. BEAUDOIN
Development Engineer
General Electric Company
Schenectady, NY 12345 USA

STEVEN M. MINER
Assistant Professor
U.S. Naval Academy
Annapolis, MD 21402 USA

RONALD D. FLACK
Professor
Department of Mechanical and Aerospace Engineering
University of Virginia
Charlottesville, VA 22901 USA

ABSTRACT

Velocity profiles were measured in the impeller of a centrifugal pump with a two directional laser velocimeter. Blade to blade profiles were measured at four circumferential positions and four radii within and one outside the four bladed impeller. Data is presented herein at two circumferential and three radial locations. The pump was tested in two configurations; with the impeller running centered within the pump, and with the impeller orbiting with a synchronous motion ($\epsilon/r_2 = 0.016$). Variation in velocity profiles among the individual passages in the orbiting impeller were found. At design flow rate, these variations ranged from 30 to 60 percent for the radial component, and 15 to 25 percent for the tangential component. Tangential velocity profiles near the impeller exit ($r/r_2 = 0.973$) were near uniform across each individual passage. Differences in the magnitude of the exit tangential velocities among the passages, however, were detected. Systematic differences in the velocity profile shapes of the centered and orbiting impellers were in general not measured, the only exception being at $r/r_2 = 0.973$ at 40% of the design flow rate. At this condition, two distinct radial velocity profiles were measured. Two of the impeller passages of the orbiting impeller contained a recirculation region covering 20–30% of the blade passage while the other two passages contained no recirculation region. The centered impeller also contained this region of reverse flow. Finally, velocity data was numerically integrated to find the forces and stiffnesses due to momentum fluxes on the impeller for the orbiting condition.

NOMENCLATURE

b	passage width
C_r	absolute radial velocity
r	radius
r_2	outer impeller radius
R_w	volute radius
Q	flow rate
Q_n	design flow rate
U_2	impeller peripheral speed
$\tilde{V}$	passage to passage velocity variation
W_θ	relative (to impeller) tangential velocity
x	horizontal direction
y	vertical direction
z	axial position from centerline
ϵ	orbit eccentricity
θ	circumferential position
ω	rotational speed
Ω	orbit speed

INTRODUCTION

Understanding and predicting the hydraulically induced force fields in any turbomachine requires detailed knowledge of the flow field. These forces can be static or dynamic (subsynchronous, synchronous, or supersynchronous). Even at design conditions, the forces can be significant and result in premature bearing failures and high operating costs, or worse, catastrophic failures with extended down times. Details of the force producing flows, however, especially for the dynamic force generators are not well known. To provide insight into hydraulic force generation this paper presents velocity measurements of the flow field in the impeller and volute of a laboratory centrifugal pump with a synchronously orbiting impeller.

A comprehensive review of the available literature on hydraulically induced forces on pump impellers is presented by Flack and Allaire (1984). A number of researchers have predicted static forces using potential flow methods. Also, several researchers have experimentally measured static forces and pressures in pumps. Recently, a few papers on experimental dynamic forces have been published.

For example, Chamieh et al. (1982), developed a test facility which allows an impeller to be orbited at speeds from anti synchronous to synchronous with the shaft speed in a standard volute type pump. They presented preliminary results for a whirl speed of 3 RPM with pump speed varying from 600 to 2000 RPM. The nondimensional force was plotted versus flow coefficient, ranging from shut off conditions to 150% of the design flow rate. The nondimensional force was not a function of pump speed at flow coefficients greater than design, but was slightly affected at lower flow coefficients. Both positive and negative whirl speeds of 3 RPM were tested with no noticeable affect on the generated force.

*Presented at the Gas Turbine and Aeroengine Congress and Exposition—June 11-14, 1990—Brussels, Belgium
This paper has been accepted for publication in the Transactions of the ASME
Discussion of it will be accepted at ASME Headquarters until September 30, 1990

More recently, Jery et al. (1985, 1984) greatly expanded the data base of impeller forces in volute type pumps. Testing was conducted by systematically varying orbit/pump speed ratio, pump speed and flow coefficient in several impeller volute combinations. The normalized, time averaged force, both normal and tangential to the impeller orbit was plotted for a given speed or flow coefficient over a range of orbit/pump speed ratios. The force was demonstrated to be proportional to the square of the pump speed. At the design flow coefficient, the radial force was found to be positive for whirl/shaft speed ratios from antisynchronous to $\Omega/\omega = 0.5$, beyond which the radial force became nominally zero. The tangential force opposed the whirling motion for all negative whirl/shaft speed ratios (a stabilizing force), but was destabilizing in the region of positive whirl speed ratios from 0 to 0.4. The nondimensional tangential force varied linearly with Ω/ω over the range tested. The tangential force did not show a great dependence on flow coefficient for flows from 70 to 160 percent of design flow. Forces at shut off condition followed the same trend over the range of whirl speeds, but were lower than other flow conditions. At the shut off condition the forces were stabilizing at all orbit/shaft speed ratios, and at the design flow coefficient the range of destabilizing forces was highest and occurred for $0 < (\Omega/\omega) < 0.5$.

Uchida et al. (1971) measured both static and dynamic radial forces on the shaft of a centrifugal pump with single volute discharge. The dynamic force component was found to be the same order of magnitude as the static component. The dominant frequencies of the dynamic force were found to be at the shaft speed and the blade pass frequency. The dynamic force was a minimum at 80% of design flow. A relative force peak occurred within the range of Q/Q_n between 0.2 and 0.4. The force increased rapidly with flow rate at flow rates above the design value. These results showed that a hydraulically induced dynamic force does exist, and it is not negligible in comparison with the static force.

Kanki et al. (1981) presented dynamic force data for four rigs. Low frequency data and blade pass frequency data was not nondimensionalized, and no balancing procedure was described. Thus, the reported synchronous component of force could be a combination of mechanical and hydrodynamic forces. The authors do show that the forces increase at low flow rates.

Although all of the papers on hydraulically generated forces are important and necessary, and they represent data which can be scaled to yield approximations to forces in other pumps, they do not indicate how the dynamic forces are generated by the flow field. Thus, the data does not indicate any means by which the dynamic performance can be improved.

A number of researchers have also studied the details of the internal flow fields in pumps. All have only studied non–orbiting impellers. For example, with the advent of laser velocimetry, a non–intrusive means of measuring velocity fields became available. Eckardt (1976, 1979) used the Laser–2–Focus method to obtain data in radially bladed, and backward swept bladed centrifugal compressors. In both cases the impellers discharged into diffusers that did not distort the impeller flow. Results showed that the velocity profile in the backward swept impeller was not as prone to separation and was more uniform at the exit.

Adler and Levy (1979), and Howard et al. (1980) used a laser–Doppler velocimeter to measure the flow in shrouded, backswept impellers. In both studies the discharge was designed not to distort the flow within the impeller. The backswept impellers showed no evidence of separation. In addition, as the fluid approached the exit, the high velocity flow shifted from the suction side to the pressure side of the blade.

Thomas et al. (1986) used laser velocimetry (LV) to measure the velocities within the logarithmic spiral volute of a laboratory centrifugal pump. A swirl generator was used to replace the impeller. Flows of 121% and 160% of design were simulated. In both cases the circumferential distribution of radial flow was nonuniform.

Mizuki et al. (1971) and Murakami et al. (1980) measured pressures and velocities within single blade passages of centrifugal impellers operating in volutes. However, no measure of the circumferential variation in flow was presented.

Kannemans (1980) used a laser–Doppler velocimeter to measure the velocity field in a radial impeller operating in a volute. Data was collected in the impeller and just outside the impeller, for one circumferential position. Circumferential variations were not considered.

Howard et al. (1987) tested three laboratory pumps. One was a single volute and the others were double volute/single discharge. They noted the effects of volute geometry on both local flow fields in the impeller and volute as well as the developed head and pressures.

Hamkins and Flack (1987) and Miner et al. (1989) used a two–directional laser velocimeter to measure the velocities within unshrouded and shrouded impellers. Impellers were concentrically operated in a logarithmic spiral volute. Data was also taken outside the impeller exit. Results showed that the flow was asymmetric, even at design flow. The asymmetries worsened as the flow rate differed from the design flow.

As summarized by the work listed here, much of the previous work in this field has focused on the impeller or the volute separately. Also, in all previous flow field studies orbiting impellers were not used. Thus, the only unsteady components of the flow were due to "blade passing" and off design conditions. Studies that have used impellers operating in volutes have concentrated on the impeller. The previous work has clearly demonstrated that the asymmetries found in impeller flows are due to the interaction between the impeller and volute. When an impeller has been operated without a volute or with a symmetric discharge region, asymmetries in the impeller flow have not been measured. However, in the case of an impeller–volute combination, circumferential variation in the impeller flow field is usually detected. Whether the flow has been above, below, or at design, these asymmetries have been measured. Therefore, in order to better understand the flow in centrifugal pumps both the impeller and volute are considered together.

The present work seeks to bridge the two pump components by providing measurements in both the impeller and volute for the same operating conditions and identify systematic variations in the flow field due to an impeller orbit. Such variations can lead to dynamic forces at the synchronous and the blade pass frequencies. The data herein lends insight to the complex flow within the impeller and its interaction with the volute. The data can also be used for verification of ongoing computational predictions of internal flows. The data presented herein is intended to complement the force data directly generated by an orbiting impeller (Chamieh et al., 1982; Jery et al., 1985, and Jery et al., 1984) and other data (Uchida et al., 1971 and Kanki, et al., 1981).

The particular objectives of the present work are to make detailed velocity measurements with a two–directional LV in both the volute and impeller of a centrifugal pump with a synchronously orbiting impeller. On design and off design conditions are studied. Blade to blade velocity profiles were to be measured for both radial and tangential velocities. These were to be obtained at different circumferential positions around

the pump. Velocity data was to be used to evaluate the synchronous forces and stiffnesses due to momentum fluxes. Axial traverses were also to be made. The pump is similar to that used in Hamkins and Flack (1987) and Miner et al. (1989) except that the impeller orbited.

EXPERIMENTAL APPARATUS

Pump

The pump used for this study is documented in Hamkins and Flack (1987) and Miner et al. (1989). The flow width (b) is 24.6 mm. The specific speed of the pump is 1583 US units which corresponds to a design flow coefficient of 0.063. Figures 1 and 2 depict the impeller and volute geometry. The impeller is a four bladed geometry with 16° logarithmic spiral blades and the volute is also a logarithmic spiral with an 83° angle. Window locations for the laser velocimeter measurements are shown in Fig. 2. The pump is constructed of Plexiglas and the casing walls are 50.8 mm thick. However, in the windows the thickness is reduced to 9.5 mm, to facilitate the use of the laser velocimeter.

For the present work the impeller is allowed to orbit. This was accomplished by offsetting the impeller center from the shaft center. Thus, the impeller orbited with the synchronous frequency ($\Omega/\omega = 1$). The orbit size was $\epsilon/r_2 = 0.016$ and the angular orientation of the impeller center to shaft center relative to a blade leading edge is shown in Fig. 3. In choosing the orbit amplitude, it should be large enough so that the synchronous velocity variations are measurable but small enough so that the tongue clearance does not change appreciably. Similar orbit sizes were used by Jery et al. (1984). The passage definitions (1 to 4) are also shown in Fig. 3.

The flow loop is shown in Fig. 4. This is a closed loop system fed from a 2000 liter reservoir tank. The flow straighteners in the 76.2 mm dia pipe upstream of the pump inlet provide a swirl free inlet flow to the pump. Static pressure taps are located 5 pipe diameters upstream of the impeller inlet and just beyond window 11 in the discharge. Yaw probe traverses in the inlet pipe indicated that the flow was swirl free three diameters upstream of the pump at shut off conditions for both orbiting and non–orbiting impellers. The second flow straightener, 9 pipe diameters upstream of the orifice flow meter, conditions the flow for the orifice plate. The globe valve is used to adjust the flow. The running speed for the pump is 620 RPM. Figure 5 shows the head–capacity curve both for the concentric operation and orbiting impeller. The design point for the present pump design is 6.3 ℓ/s at 0.178 x 10^5 N/m^2. This design point is based on an estimate of the impeller–volute matching point. The matching point is the condition which causes the average angular momentum of the flow at the impeller exit to equal the average angular momentum in the throat of the volute.

Laser Velocimeter

The laser and optics for this system are shown in Fig. 6. The system is 3–beam frequency shifted, operated in the forward scatter mode. The Bragg cell performs the dual functions of beam separation and frequency shifting. A single primary beam enters the cell and the primary beam and an orthogonal grid of secondary beam emerges. However, only three of the beams are used, the primary beam and two secondary beams. The secondary beams are shifted by different frequencies. These three beams form a 90° angle. Therefore, when the beams are focused and crossed at the probe volume two sets of perpendicular interference fringes are created. These two sets of fringes allow the simultaneous measurement of two orthogonal components of velocity. The entire optical system was mounted on a three directional traversing mechanism with

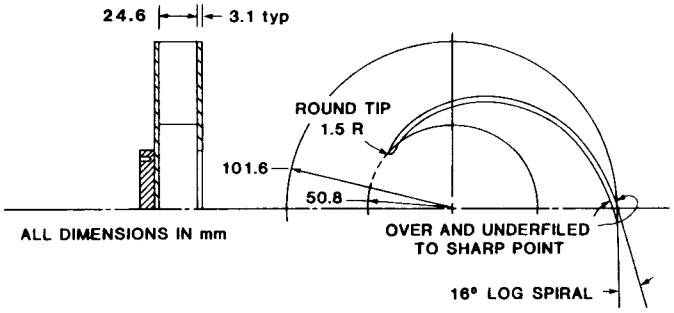

Fig. 1 Impeller Geometry

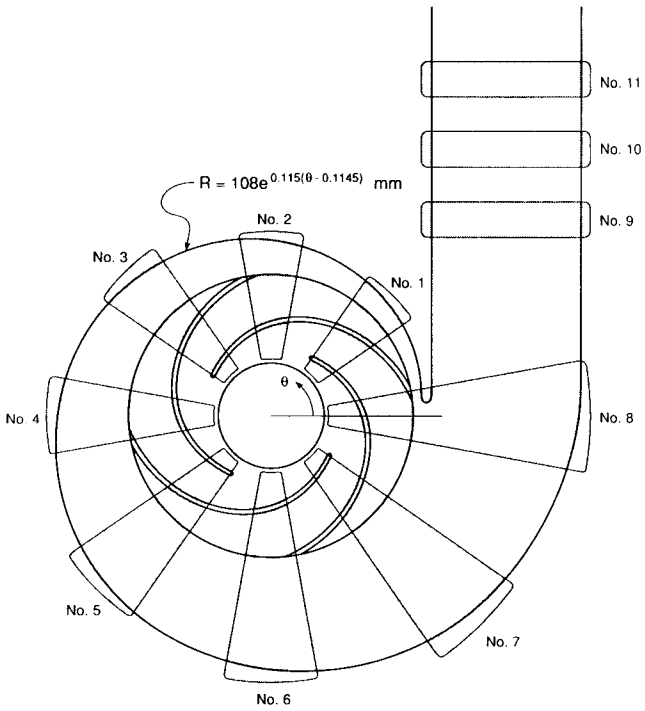

Fig. 2 Volute and Window Location

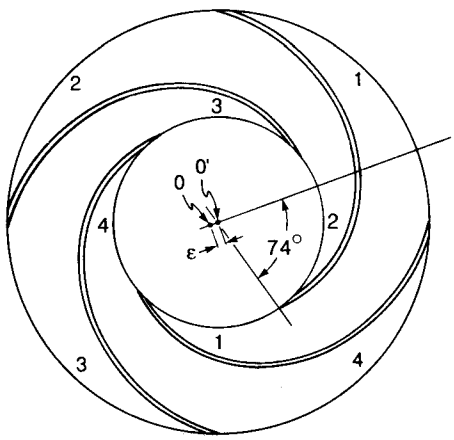

0' = Impeller Center
0 = Shaft Center

Fig. 3 Impeller Eccentricity Orientation and Passage Definition

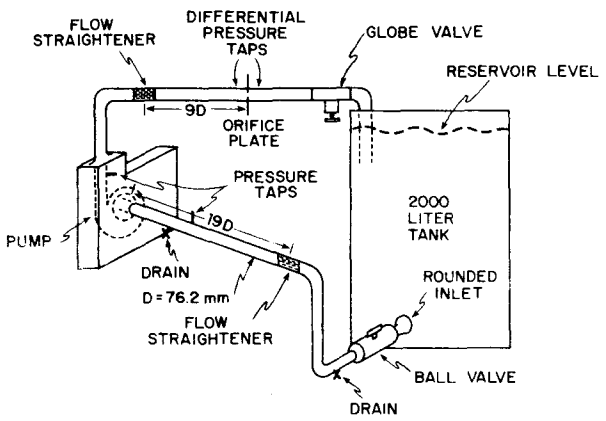

Fig. 4 Flow Loop

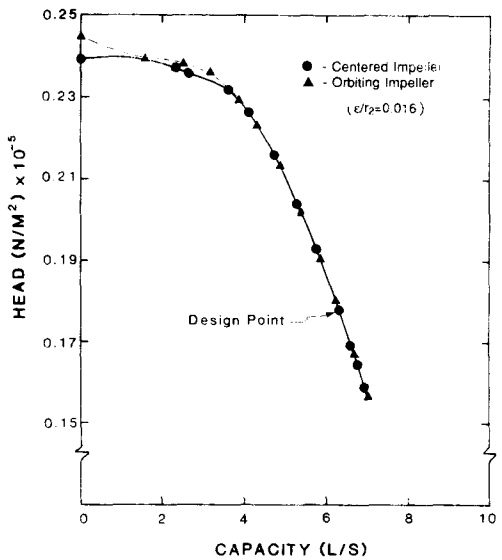

Fig. 5 Pump Head – Capacity Curves

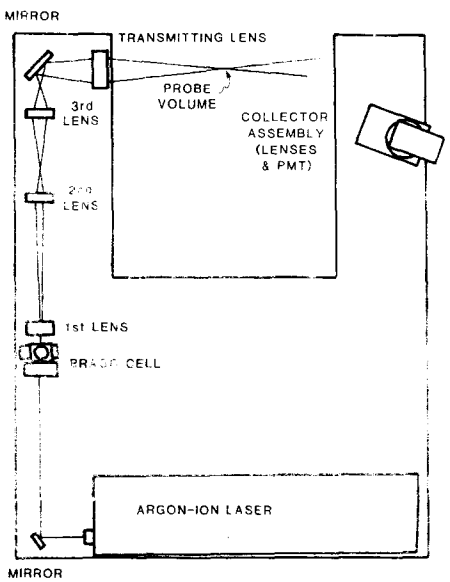

Fig. 6 LV System

digital position readouts. The probe volume was easily and accurately moved in the x, y and z directions with this mechanism.

The frequency of light scattered from the probe volume determines the velocity. Light was scattered by naturally occurring particles in the water. The water was filtered, using a taste and odor filter. This provided particles of 5 μm and smaller. Two burst type signal processors with adjustable threshold and five/eight count comparison with adjustable tolerances were used. Signals from both sets of beams are checked for coincidence. If the signals occur at the same time, then they are considered valid.

Once a valid LV signal is generated, the impeller angular position is recorded with a shaft encoder. The encoder divides each revolution into 256 parts. The two velocity signals and the shaft position are simultaneously recorded onto floppy disks by a dedicated microcomputer. A typical test had 5000 data points, approximately 20 per each of the 256 "shaft angle bins". This gave 2–D velocity and angular position data for the four blade passages, which was analyzed after the test.

Uncertainty

The uncertainty in probe volume position was 0.5 mm radially and 1 mm axially. The uncertainty in the angular position was 0.30°. The uncertainty in the angular orientation of the probe volume fringes with respect to the reference axes was 0.85°. This was the dominant factor in flow direction uncertainty. The typical uncertainty in the radial velocity component was 0.04 m/sec and the typical uncertainty in the tangential velocity component was also 0.04 m/sec. These velocity uncertainties do not include the effect of positional uncertainty in the presence of velocity gradients. The position of the probe volume is uncertain, particularly in the axial direction. Since spatial velocity gradients are present, a misplaced probe volume will measure the incorrect velocity. This spacial uncertainty results in a total uncertainty of 0.10 m/sec for the radial velocity and also 0.10 m/sec for the tangential velocity.

When examining the differences between the different blade to blade profiles for the orbiting impeller data, one only has to consider the affect of random uncertainty. For these cases the data was recorded without moving the probe volume and thus data was acquired for exactly the same probe volute location. The uncertainty due to the axial gradient, however, must be considered when comparing the profiles for the centered and orbiting impeller passages, since this data was recorded at different times, and the probe volume location was not exactly the same for the two sets of data (due to positional uncertainty).

RESULTS

Experimental data for this study were taken in windows 1, 4, 6, and 8. For each window, data was taken at four radial positions within the impeller. Volute data in window 1 was taken at only [illegible] data at six radial volute positions were taken in each of the other three windows. These data were taken at [illegible] of the design flow of 6.3 l/s. In addition, data for five flow rates were taken in window 6 at the axial centerline. Representative results are presented here and are nondimensionalized by the impeller tip velocity. Data at other axial locations were taken but are not presented here in the sake of brevity. Results are presented in the form of fourth order polynomial least squares curve fits to the average velocity data profiles. The symbols are used only as a means of identifying the curves and do not represent actual data. In general, data is presented for the four different passages and compared to the non–orbiting impeller data.

Complete presentation and discussion of the results can be found in Beaudoin (1987) and Miner (1988).

Figure 7 contains the passage averaged profiles of all four passages for both the orbiting and centered impeller cases for a typical test run (window 6, $r/r_2 = 0.973$, $Q/Q_n = 1.00$). The two impeller conditions have similar profile shapes for both the radial and tangential velocities. There are, however, differences in the magnitudes of the profiles. These are due to uncertainty in the probe volume position (as shown) in addition to the differences in the data between the centered and orbiting impellers due to the unsteady nature of the flow.

Next, typical impeller data for variations in radius and circumferential position are presented to demonstrate the passage to passage variations. These are presented in Figs. 8 through 11 for two radius ratios and two circumferential positions. When comparing velocity data for the passages the uncertainty is much smaller as indicated in Fig. 8. It is important to note that the different passage data for the non–orbiting impeller fell within the small uncertainty band indicated in Fig. 8. This data is not presented for the sake of brevity.

At a radius ratio of 0.625 (Figs. 8 and 9, windows 1 and 6) passage 4 tended to have the highest radial velocity across the central portion of the passage span. Variations in velocities in midstream and near the blade surfaces, particularly the suction surface are systematic, i.e. one can see a repetitive pattern. For example, for the midspan portion of C_r/U_2 for Window 1 (Fig. 8) one can see the velocity varies from $C_r/U_2 = 0.135$ to 0.085 to 0.090 to 0.155 and back to 0.135 as the impeller varies from passage 1 to 2 to 3 to 4 and back to 1. Such periodicity is seen on most profiles. Passage 1 had the second highest radial velocity values at each of the four circumferential positions tested. All the radial profiles were skewed toward the suction surface, with the profile peak values occurring in the range of 80% of the passage span.

Tangential profiles show passage 4 to have the highest relative tangential velocity, i.e. lowest absolute velocity, in the central portion of the blade span at each circumferential position. Passage 2 had the lowest relative tangential velocity in each of the four cases. One should again note a systematic variation in the blade to blade profile on these figures.

In Figs. 10 and 11 data for a radius ratio of 0.973 is presented for windows 1 and 6. Variations in the radial profiles are now more symmetric than profiles measured at the smaller radii, with equal peaks at the suction and pressure surfaces, with the lowest value near mid span. Near the impeller exit for all conditions the largest passage to passage fluctuations occured in Window 1 (Fig. 10). In this region the impeller/volute clearance is smallest, indicating that this varying clearance strongly influences the flow field in the impeller.

For a radius ratio of 0.973 the tangential profiles are nearly uniform across the passage up to 80% span where the relative velocity becomes small. Absolute tangential velocity data for radius ratios 0.875 (data not shown) to 0.973 (Figs. 10 and 11) indicates that very little additional rotational energy is added to the flow between these radius ratios in the region from pressure surface to midspan. Passage 2 consistently demonstrated the highest absolute tangential velocity (lowest relative tangential velocity) across the span and passage 4 showed the lowest absolute velocity as measured at the four circumferential probe volume locations. Thus, the lowest relative tangential velocity was in the passage that lagged (by approximately 90°) the minimum impeller/volute clearance.

Typical measurements in the volute near the impeller exit are presented in Fig. 12 (window 6, $r/r_2 = 1.028$). These measurements were made in the volute, from nondimensional

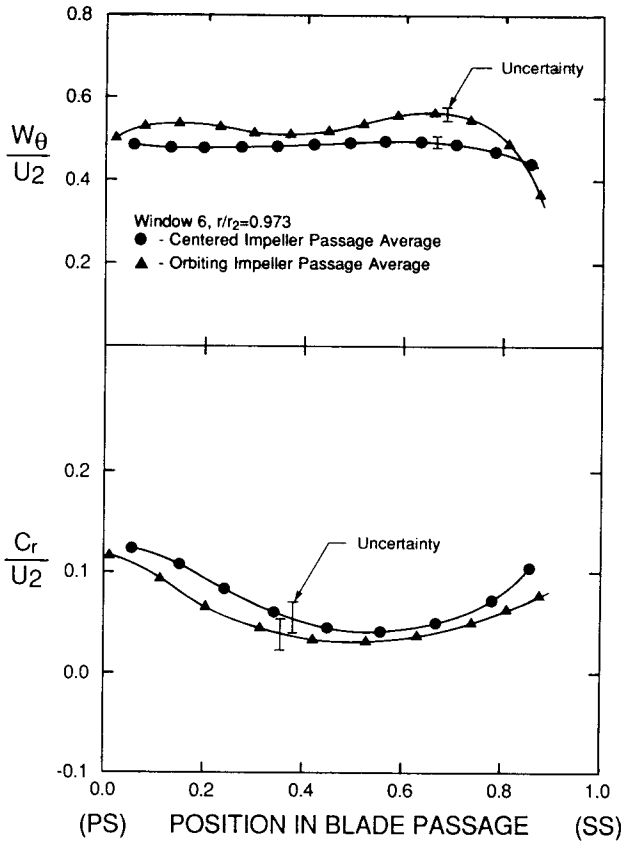

Fig. 7 Passage Averaged Velocity Profiles – Centered and Orbiting Impellers (Window 6, $r/r_2 = 0.973$, $Q/Q_n = 1.00$)

distances of 0.012 to 0.043 from the impeller exit, depending on the circumferential location relative to the eccentricity. Passages 1 and 2 tended to have a wider peak to peak variation in the radial profile. All the passage profiles had maximum values at 20% of the blade "span". The measurements are made outside of the impeller, so the angular locations of the blade tips at the impeller exit are used to bracket the profiles.

By examining Figs. 10, 11 and 12 ($r/r_2 = 0.973$ and 1.028) one can see that differences between the nondimensional velocity profiles for passages 2 and 4 ranged from 0.05 to 0.14 in the central portion of the blade span. Systematic periodic trends among the radial velocity profiles are again observed at these radii. Although the data are similar they are not within the uncertainty which is indicated in Fig. 8.

Tangential velocity profiles show passage 2 to have the highest absolute velocity of the four orbiting passages for the majority of the span at three of the four circumferential positions tested, the exception being window 8. Passage 4, on the average, had the lowest absolute tangential velocities.

Flow variation studies were conducted in window 6 at radii ratios of 0.625 and 0.973. Figures 9 and 13 through 16 are for $r/r_2 = 0.625$ and show the passage to passage comparison for the orbiting impeller for the range of flows tested. In general passage 4 had the highest radial peak velocity of the four orbiting passages for all tested flow rates, while passage 2 had the lowest peak value. As with the centered impeller profiles (Miner et al., 1989), orbiting passage radial peak values were located at 80% of span, the exception being at $Q/Q_n = 0.4$. The absolute tangential velocity along a passage profile varied inversely to radial velocity for all the passages at all flow rates except $Q/Q_n = 0.4$.

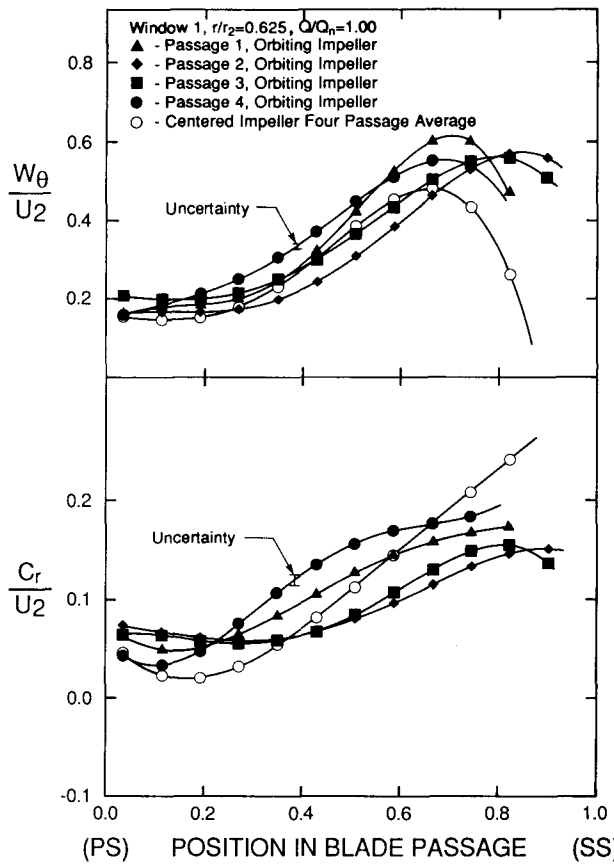

Fig. 8 Velocity Profiles (Window 1, $r/r_2 = 0.625$, $Q/Q_n = 1.00$)

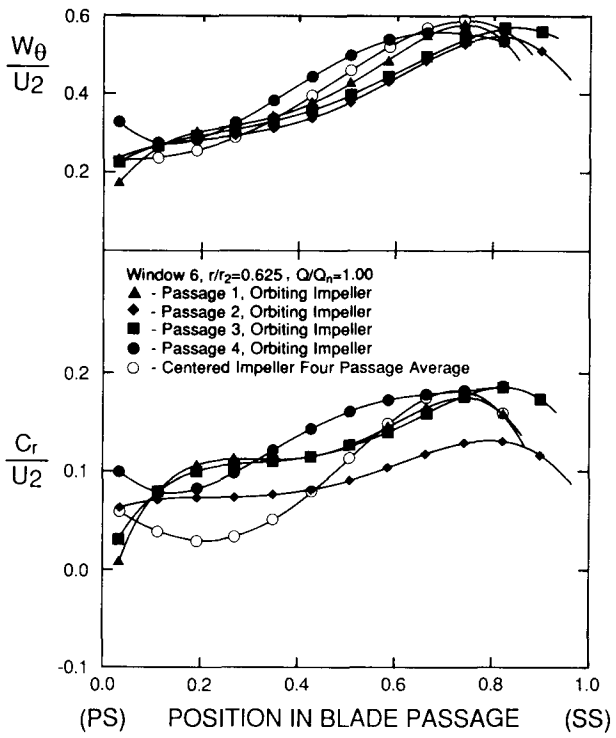

Fig. 9 Velocity Profiles (Window 6, $r/r_2 = 0.625$, $Q/Q_n = 1.00$)

The orbiting impeller radial velocity profiles at $r/r_2 = 0.973$ (Figs. 10 and 17 through 20) have the same basic shapes for flow rates from 60 to 106% of design flow. Peak values are present on the two blade surfaces with the minimum value near midspan. At $Q/Q_n = 0.4$ (Fig. 17) two distinct profile shapes are seen; passages 1 and 4 have two relative maximums (at 10 and 80% of span) and relative minimums at 50% span and negative velocities near the suction surface. Passages 2 and 3, and the centered impeller profiles are highest on the pressure surface and have pronounced minimums which vary in location from 60 to 80% of span depending on the passage and with negative velocities which vary in span length from 16 to 28%.

Tangential velocity profiles show a change from an essentially flat profile across the span at 100 and 106% of design flow to a profile, where turning is increased along the span from pressure side to suction side for low flow rates. At $Q/Q_n = 0.4$ the profiles fluctuate along the span. Passages 1 and 3 have profiles where the relative tangential velocity decreases markedly from 60% span to the blade suction surface.

To summarize the passage to passage variations due to the orbiting operation, Table 1 is presented. This table shows the mean variation among the four individual passage profiles of the orbiting impeller for both velocity components. The variation is defined by:

$$\bar{\nabla} \equiv \frac{2}{\pi} \int_0^{\pi/2} \frac{\Delta G(\theta)}{G(\theta)} \, d\theta$$

where ΔG and G are illustrated in Fig. 20 and where

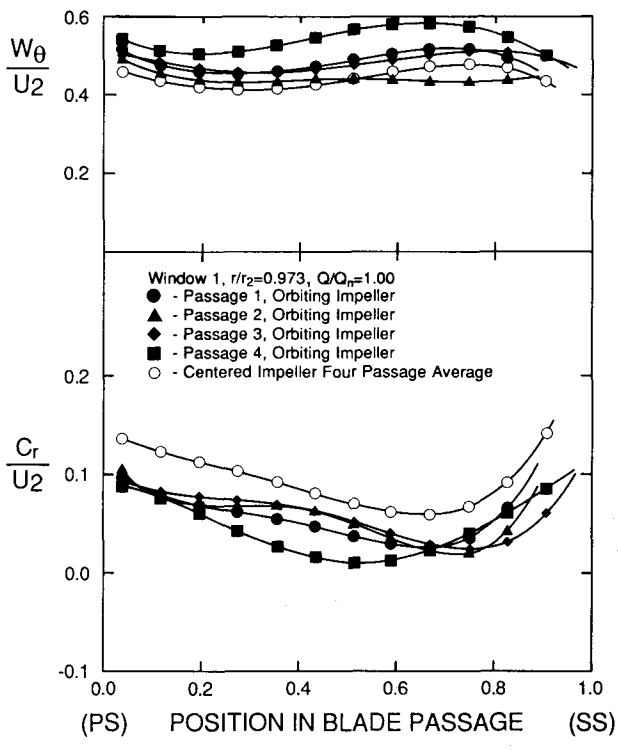

Fig. 10 Velocity Profiles (Window 1, $r/r_2 = 0.973$, $Q/Q_n = 1.00$)

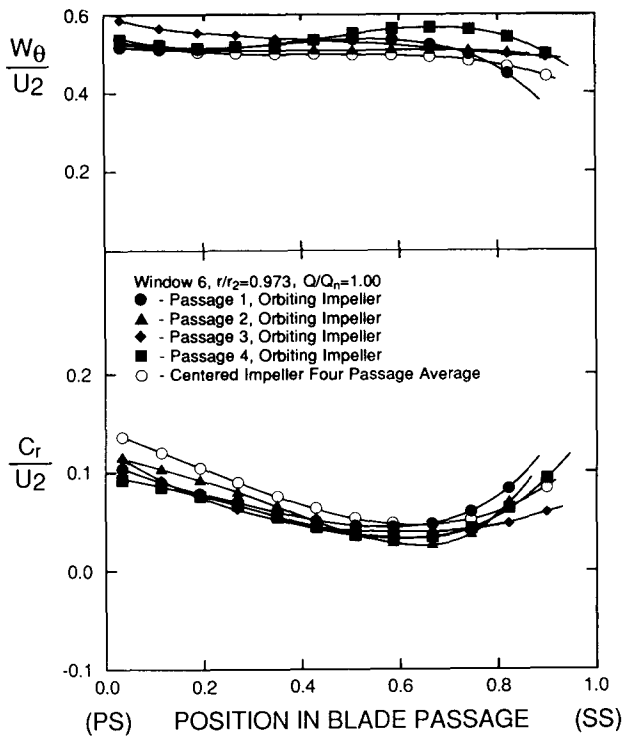

Fig. 11 Velocity Profiles (Window 6, r/r_2 =0.973, Q/Q_n =1.00)

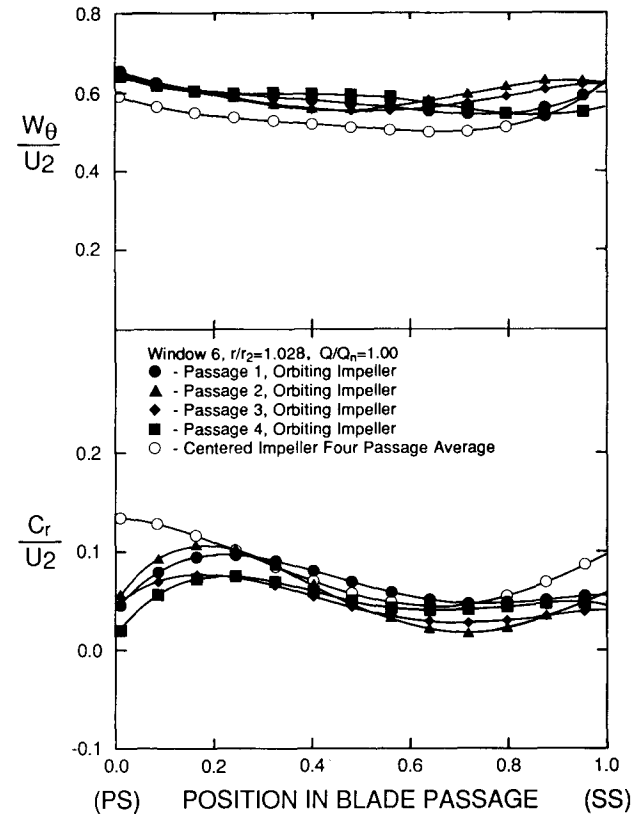

Fig. 12 Velocity Profiles (Window 6, r/r_2 =1.028, Q/Q_n =1.00)

Table 1 Variation in Blade to Blade Velocity Profiles in Orbiting Impeller ($\epsilon = e/r_2 = 0.016$)

r/r_2	Window	Q/Q_n	$\tilde{V}_r$	$\tilde{W}_\theta$
0.625	1	1.00	0.30	0.20
0.625	4	1.00	0.30	0.25
0.625	6	1.00	0.40	0.20
0.625	8	1.00	0.50	0.20
0.75	1	1.00	0.40	0.15
0.75	4	1.00	0.55	0.20
0.75	6	1.00	0.30	0.15
0.75	8	1.00	0.45	0.15
0.875	1	1.00	0.35	0.20
0.875	4	1.00	0.50	0.15
0.875	6	1.00	0.30	0.20
0.875	8	1.00	0.40	0.15
0.973	1	1.00	0.60	0.20
0.973	4	1.00	0.50	0.10
0.973	6	1.00	0.30	0.10
0.973	8	1.00	0.35	0.15
1.028	1	1.00	0.55	0.05
1.028	4	1.00	0.75	0.05
1.028	6	1.00	0.50	0.05
1.028	8	1.00	0.90	0.05
0.625	6	0.40	1.80	0.25
0.625	6	0.60	0.90	0.30
0.625	6	0.80	0.60	0.30
0.625	6	1.00	0.40	0.20
0.625	6	1.06	0.50	0.15
0.973	6	0.40	2.50	0.40
0.973	6	0.60	0.40	0.10
0.973	6	0.80	0.40	0.05
0.973	6	1.00	0.30	0.10
0.973	6	1.06	0.30	0.10

ΔG – maximum variation among profiles at a given span location
G – mean value of profiles at a given span location
θ – span location

From this table three trends can be seen. First, the passage to passage variation for the radial component increases with increasing radius. In fact the largest fluctuations occur in the volute at a radius ratio of 1.028. Second, the trend is the opposite for the tangential component, namely this variation decreases with increasing radius; the smallest variation occurs in the volute. Third, near the impeller periphery the largest fluctuations in radial velocity occur near the tongue indicating that the tongue clearance influences the flow rate in the adjacent passage. And fourth, when examining the different flow rates, one sees that the largest variations for both components occur at off–design conditions. At the design flow rate, the radial velocity profiles had passage to passage variations from 30 to 60 percent of the mean value. The relative tangential velocity profiles had variations from 15 to 25 percent at design condition. At 40% flow the variations are as much as eight times the variations at design conditions. This implies that at low flow rates synchronous forces (and noise) and multiples thereof will be largest. This has in fact been found to be the case as reported by Uchida et al. (1971) and Kanki et al. (1981). Internal flow measurements are now available to help explain why these forces are generated.

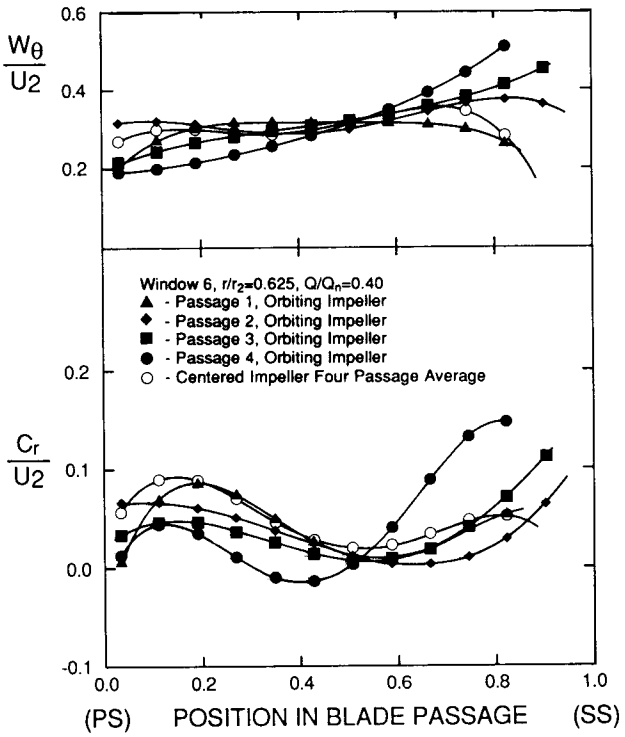

Fig. 13 Velocity Profiles (Window 6, r/r_2 =0.625, Q/Q_n =0.40)

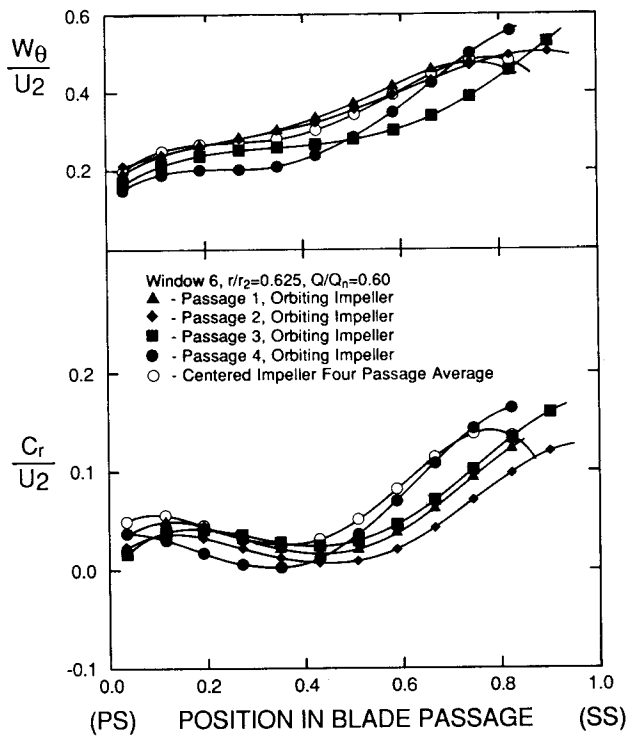

Fig. 14 Velocity Profiles (Window 6, r/r_2 =0.625, Q/Q_n =0.60)

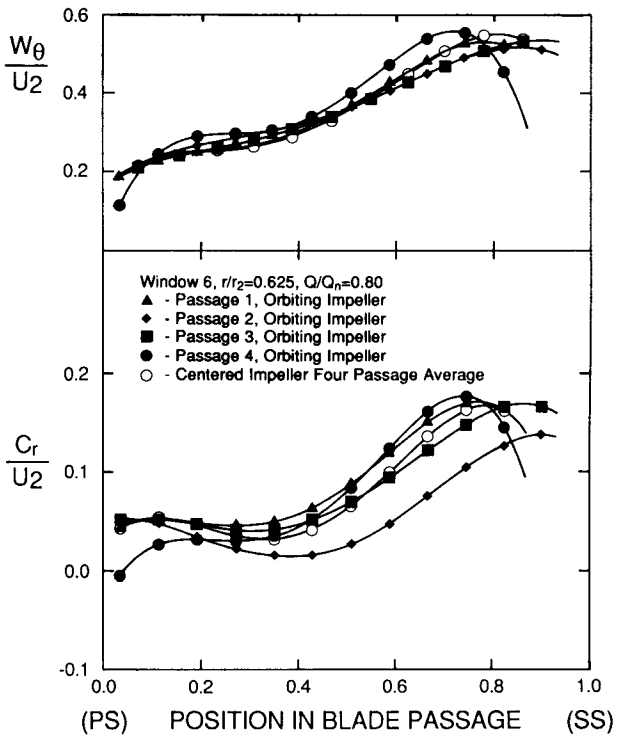

Fig. 15 Velocity Profiles (Window 6, r/r_2 =0.625, Q/Q_n =0.80)

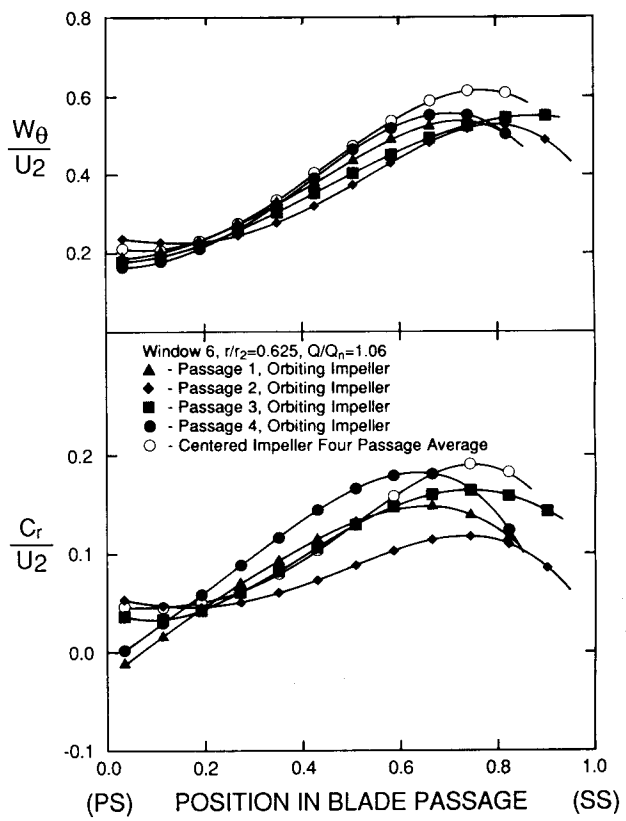

Fig. 16 Velocity Profiles (Window 6, r/r_2 =0.625, Q/Q_n =1.06)

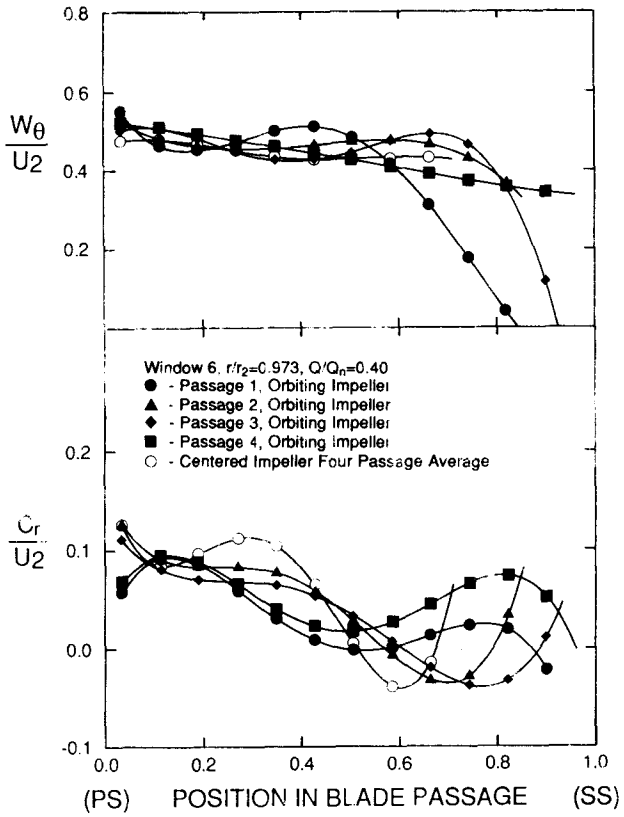

Fig. 17 Velocity Profiles (Window 6, r/r_2 =0.973, Q/Q_n =0.40)

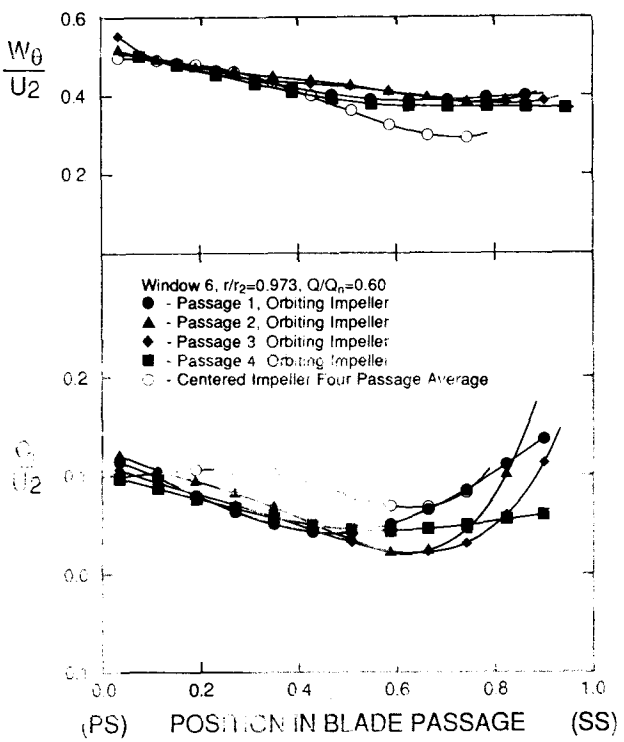

Fig. 18 Velocity Profiles (Window 6, r/r_2 =0.973, Q/Q_n =0.60)

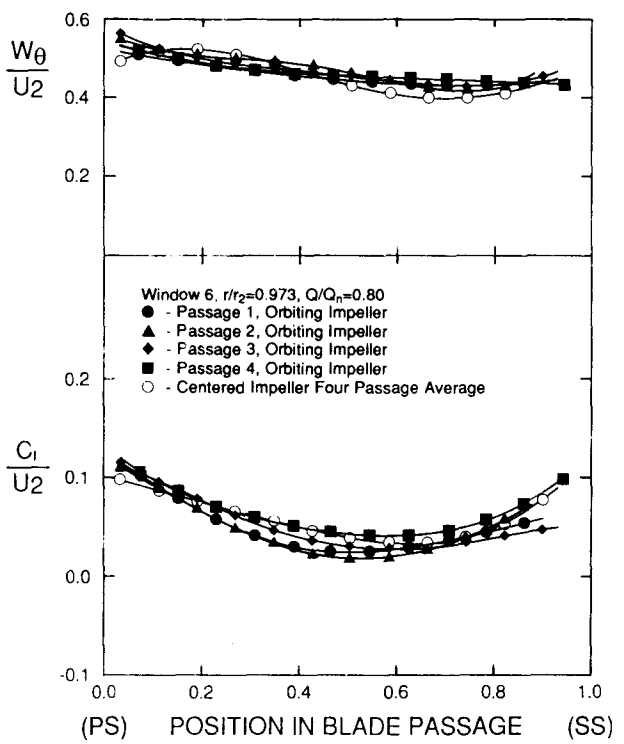

Fig. 19 Velocity Profiles (Window 6, r/r_2 =0.973, Q/Q_n =0.80)

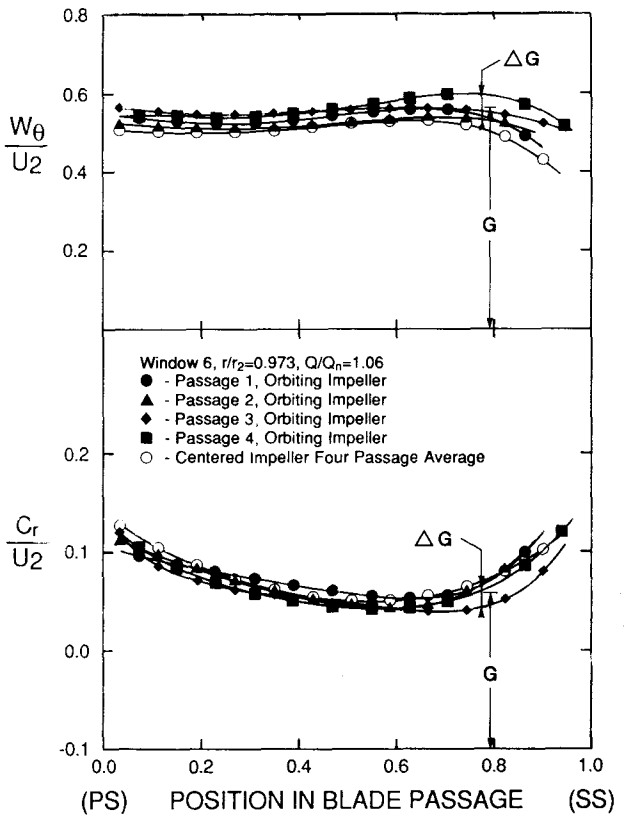

Fig. 20 Velocity Profiles (Window 6, r/r_2 =0.973, Q/Q_n =1.06)

To summarize a portion of the velocity data into such forces, one can numerically integrate the momentum fluxes at the exit of the impeller. Allaire et al. (1984) showed that for pumps of this scale with an unbounded volute the predominant force on the impeller results from the momentum fluxes as opposed to the pressure forces. By numerically integrating the velocities around the impeller exit for one impeller angular orientation (i.e., position in the orbit) one can find the force vector due to momentum fluxes at that impeller position:

$$\vec{F} = \int \vec{V}\, \rho\, \vec{V} \cdot d\vec{A}$$

$$\simeq \sum_{\theta=0}^{360^\circ} \vec{V}\, \rho\, C_r\, r_2\, \Delta\theta$$

By finding the periodic fluctuating forces due to the orbit one can find the stiffnesses by:

$$K_{xx} = -\Delta F_x/\Delta x \qquad K_{yy} = -\Delta F_y/\Delta y$$

$$K_{yx} = -\Delta F_y/\Delta y \qquad K_{xy} = -\Delta F_x/\Delta y$$

For example, one finds K_{xx} when the impeller position is $\Delta x = \pm \epsilon$ and $\Delta y = 0$, and evaluates ΔF_x as the difference between the x–component of force at this position and the average x–force. One can nondimensionalize these by

$$\bar{K}_{ij} = K_{ij}\, r_2/[1/2\, \rho\, A_2\, U_2^2]$$

where $A_2 = 2\pi r_2 b$.

The above numerical integration was carried out for design flow conditions for four impeller positions and the synchronous results are presented in Table 2. As can be seen, the stiffnesses are not symmetric, i.e. $\bar{K}_{xx} \neq \bar{K}_{yy}$ and $\bar{K}_{xy} \neq \bar{K}_{yx}$. This is due to the nonsymmetry of the volute and the fact that the tongue clearance changes as the impeller orbits. One should also note that the magnitudes of the stiffnesses are of the same order as predicted by Allaire et al. (1984) and measured by Jery et al. (1984) for similar but not identical sized pumps. Of particular importance is the negative sign on K_{xx} as also reported in Allaire et al. (1984) and Jery et al. (1984) indicating a destabilizing mechanism.

Table 2 Nondimensional Stiffnesses for Design Flow Due to Momentum Fluxes

$\bar{K}_{xx}$	-0.161
$\bar{K}_{yy}$	-0.005
$\bar{K}_{yx}$	-0.029
$\bar{K}_{xy}$	0.229

CONCLUSIONS

The measurement of fluid velocities in the impeller of a single volute type pump were made in two pump configurations: (i) with the impeller running centered and (ii) with a whirling motion on the impeller which was induced by offsetting the impeller center from the shaft center. Blade to blade velocity profiles were generated as the impeller rotated through an LV probe volume located at various fixed positions in the pump. Comparisons were made both between the individual passage profiles of the orbiting impeller and to the four passage average profile of the centered impeller.

The average variations among the individual passage velocity profiles in the orbiting impeller were calculated for each test conducted. At the design flow rate, the radial velocity profiles had passage to passage variations from 30 to 60 percent of the mean value. The relative tangential velocity profiles had variations from 15 to 25 percent at design condition. Passage to passage variations were systematic and periodic as the four flow passages swept by the fixed measurement location. At off–design conditions the variation in radial velocity profiles increased by as much as eight times as flow rate decreased. Such increases in velocity variations imply increased momentum variations which result in increased dynamic forces, as have been previously measured and reported. The current data represent the first internal velocity data to complement the force measurements.

Next, the passage to passage variation for the radial component was seen to increase with increasing radius. In fact the largest fluctuations occurred in the volute. This trend was the opposite for the tangential component. Namely, this variation decreased with increasing radius and the smallest variation occured in the volute.

At radius ratios of 0.973 and 1.028 the tangential velocity profiles were relatively flat across the individual blade passages. Systematic variations of the velocity levels of the different passages were measured, however. Passage 2 contained the highest absolute tangential velocities of the four orbiting passages while passage 4 contained the lowest velocities. Differences between the nondimensional velocity profiles for passages 2 and 4 ranged from 0.05 to 0.14 in the central portion of the blade span. At the impeller exit the largest fluctuations were seen in Window 1, which is adjacent to the tongue (smallest clearance area).

At a radius ratio of 0.625 at the design flow rate, absolute tangential velocity was found to be inversely related to radial velocity both for a given passage along the span, and among the four passages at a given span location in the central portion of the blade span. Passage 4 had the highest radial values and lowest absolute tangential values. This trend was also true at tests conducted at a radius ratio of 0.750, but not at the larger radii in the impeller.

At the off–design flow rate of $Q/Q_n = 0.4$, two distinct radial velocity profiles were measured at a radius ratio of 0.973. The radial velocity profile of the centered impeller and passages 2 and 3 of the orbiting impeller contained regions of negative velocity covering 16 to 28 percent of the passage span. The recirculation zones were located from 60% to 80% of the passage span. Passage 1 and 4 profiles contained negative velocities near the suction surface (100 percent passage span) but had relative maxima at both 10 and 80 percent passage span. Such systematic variations in profile shapes among the passages were not measured at a radius ratio of 0.625 at $Q/Q_n = 0.4$.

To demonstrate use of the data the velocity momentum profiles were numerically integrated around the impeller periphery at the design flow rate. This resulted in fluctuating forces due to fluctuating momentum fluxes. Using these force variations, stiffnesses were found. These were found to be of the same order of magnitudes as found previously both theoretically and experimentally for similar sized pumps.

ACKNOWLEDGEMENT

This research was sponsored by the Rotating Machinery and Controls (ROMAC) Industrial Research Program at the University of Virginia.

REFERENCES

Adler, D., Levy, Y., "A Laser–Doppler Investigation of the Flow Inside a Backswept, Closed, Centrifugal Impeller," Journal of Mechanical Engineering Science, Vol. 21, No. 1, 1979, pp. 1–6.

Allaire, P. E., Sato, C. J., and Branagan, L. A., "Hydraulic Forces on a Centrifugal Impeller Undergoing Synchronous Whirl," Rotordynamic Instability Problems in High–Performance Turbomachinery, NASA CP–2338, May 1984, pp. 123–136.

Beaudoin, R. J., "Laser Velocimetry Measurements in a Centrifugal Pump with an Orbiting Impeller," M.S. Thesis, University of Virginia, December 1987.

Chamieh, D. S., Acosta, A. J., Brennen, C. E., Caughy, T. K., and Franf, R., "Experimental Measurements of Hydrodynamic Stiffness Matrices for a Centrifugal Pump Impeller," Workshop on Rotordynamic Instability Problems in High Speed Turbomachinery, Texas A&M University, NASA CP 2250, May 1982, pp. 382–398.

Eckardt, D., "Detailed Flow Investigations within a High Speed Centrifugal Compressor Impeller," Trans. ASME, Journal of Fluids Engineering, Vol. 98, No. 3, September 1976, pp. 390–402.

Eckardt, D., "Flow Field Analysis of Radial and Backswept Centrifugal Compressor Impellers, Part 1: Flow Measurements Using a Laser Velocimeter," Performance Prediction of Centrifugal Pumps and Compressors, ASME I00127, 1979, pp. 77–86.

Flack, R. D., and Allaire, P. E., "Lateral Forces on Pump Impellers – A Literature Review," The Shock and Vibration Digest, Vol. 16, No. 1, January 1984, pp. 5–14.

Hamkins, C. P., Flack, R. D., "Laser Velocimeter Measurements in Shrouded and Unshrouded Radial Flow Pump Impellers," ASME Trans., Journal of Turbomachinery, Vol. 109, No. 1, January 1987, pp. 70–76.

Howard, J. H. G., Mukker, O. S., Naoem, T., "Laser Doppler Measurements in a Radial Pump Impeller," Measurement Methods in Rotating Components of Turbomachinery, ASME I00130, 1980, pp. 133–138.

Howard, J. H. G., Abramian, M. and Hermann, P., "Experimental Investigation of Impeller and Volute Flow Fields for a Low Specific Speed Pump with Single and Double Volutes," Proceedings of the 1987 ASME/JSME Thermal Engineering Joint Conference, Vol. 2, pp. 51–61.

Jery, B., Acosta, A. J., Brennen, C. E., and Caughy, T. K., "Hydrodynamic Impeller Stiffness, Damping, and Inertia in Rotordynamics of Centrifugal Flow Pumps," Proceedings of the Workshop on Rotordynamic Instability Problems in High Performance Turbomachinery, Texas A&M University, May 1984, NASA–CP2338, pp. 137–160.

Jery, B., Brennen, C. E., Caughy, T. K., and Acosta, A., "Forces on Centrifugal Pump Impellers," Proceedings of the Second International Pump Symposium, Texas A&M University, College Station, TX, 1985, pp. 21–29.

Kanki, H., Kawata, Y., and Kawatani, T., "Experimental Research on the Hydraulic Excitation Force on the Pump Shaft," ASME Paper No. 81–DET–71, 1981.

Kannemans, H., "Radial Pump Impeller Measurements Using a Laser Doppler Velocimeter," ASME Paper No. 80–GT–94, 1980.

Miner, S. M., "Potential Flow Analysis of a Centrifugal Pump: Comparison of Finite Element Calculation and Laser Velocimeter Measurement," Ph.D. Dissertation, University of Virginia, Dept. of Mechanical & Aerospace Engr., January 1988.

Miner, S. M., Beaudoin, R. J., and Flack, R. D., "Laser Velocimetry Measurements in a Centrifugal Flow Pump," ASME Trans., Journal of Turbomachinery, Vol. 111, No. 3, July 1989, pp. 205–212.

Mizuki, S., Sakai, T., Watanabe, I., "A Study of the Flow Pattern within the Centrifugal and Mixed–Flow Impellers," ASME Paper No. 71–GT–41, 1971.

Murakami, M., Kikuyama, K., Asakura, E., "Velocity and Pressure Distributions in the Impeller Passages of Centrifugal Pumps," ASME Trans., Journal of Fluids Engineering, Vol. 102, No. 4, December 1980, pp. 420–426.

Thomas, R. N., Kostrzewsky, G. J., Flack, R. D., "Velocity Measurements in a Pump Volute with a Non–Rotating Impeller," Int. J. Heat and Fluid Flow, Vol. 7, No. 1, March 1986, pp. 11–20.

Uchida, N., Kenasku, I., and Shirai, I., "Radial Forces on the Impeller of a Centrifugal Pump," Bulletin JSME, Vol. 14, No. 76, 1971, pp. 1106–1117.